

# ⚠️OMNIVIEW: An All-Seeing Diffusion Model for 3D and 4D View Synthesis

Xiang Fan<sup>1,2</sup> Sharath Girish<sup>2</sup> Vivek Ramanujan<sup>1</sup> Chaoyang Wang<sup>2</sup> Ashkan Mirzaei<sup>2</sup>  
 Petr Sushko<sup>1</sup> Aliaksandr Siarohin<sup>2</sup> Sergey Tulyakov<sup>2</sup> Ranjay Krishna<sup>1</sup>

<sup>1</sup>University of Washington <sup>2</sup>Snap Inc.

Project page: <https://snap-research.github.io/OmniView>

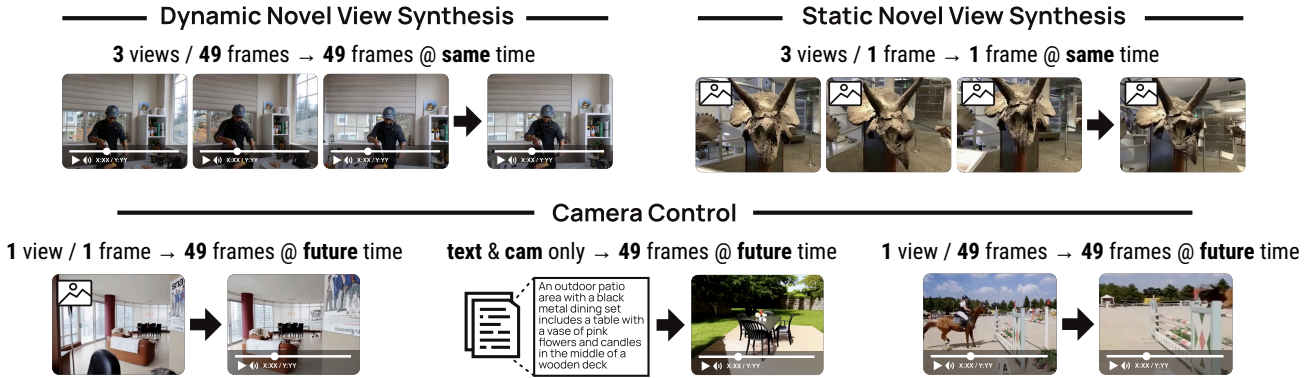


Figure 1. **OMNIVIEW**: Given one or more images or videos, captured at potentially different viewpoints and times, OMNIVIEW generates 4D-consistent videos that can be rendered from novel camera trajectories, viewpoints, times, and durations. OMNIVIEW unifies many existing video generation paradigms, enabling tasks such as novel view synthesis (NVS), text-to-video (T2V) camera control, and multi-view conditioning in one model.

## Abstract

Prior approaches injecting camera control into diffusion models have focused on specific subsets of 4D consistency tasks: novel view synthesis, text-to-video with camera control, image-to-video, amongst others. Therefore, these fragmented approaches are trained on disjoint slices of available 3D/4D data. We introduce OMNIVIEW, a unified framework that generalizes across a wide range of 4D consistency tasks. Our method separately represents space, time, and view conditions, enabling flexible combinations of these inputs. For example, OMNIVIEW can synthesize novel views from static, dynamic, and multiview inputs, extrapolate trajectories forward and backward in time, and create videos from text or image prompts with full camera control. OMNIVIEW is competitive with task-specific models across diverse benchmarks and metrics, improving image quality scores among camera-conditioned diffusion models by up to 33% in multiview NVS LLFF dataset, 60% in dynamic NVS Neural 3D Video benchmark, 20% in static camera control on RE-10K, and reducing camera trajectory errors by 4x in text-conditioned video generation. With strong general-

izability in one model, OMNIVIEW demonstrates the feasibility of a generalist 4D video model.

## 1. Introduction

When trained on raw internet-scale video, video diffusion models internalize strong 3D priors [34, 44, 58]. They can synthesize long, coherent camera motions and maintain scene layout without any explicit geometry [48]. Yet, by default, they offer little explicit 3D control. To deploy them in applications such as virtual/augmented reality, film production, robotics, or autonomous driving, they need to be controllable. Many applications would become possible if we could control how the generator’s camera moves in space and in time. Naturally, this motivation has driven multiple sub-fields of computer vision to develop specialized solutions. Camera redirection now exists for multi-view static [18, 91] and dynamic Novel View Synthesis (NVS) [4, 61], text-to-video (T2V) [21, 78] and image-to-video (I2V) [74] with camera control, and even video-to-video (V2V) [5].

However, existing approaches are fragmented along task, architecture, and data. Methods designed for multi-view static NVS focus on reconstructing a single scene from sparse views [91], achieving strong 3D consistency but only at a fixed timestamp, and thus cannot handle dynamic videos. Camera-control T2V/I2V models convert text or a single image plus a camera trajectory and generate a moving video, but their architectures cannot ingest full input videos [21]. V2V redirection models accept a source video and re-render it from a new camera path at matched timestamps, yet they typically cannot operate in the multi-view setting [5]. Some works rely on explicit geometric representations (depth maps, point clouds, or other 3D/4D fields) for consistency [51, 70, 83, 85], rather than exploiting the implicit 3D priors already present in video models.

Because each family of methods is tailored to a narrow I/O configuration, they are trained on disjoint slices of available 3D/4D data, leaving most geometric supervision unused. We argue that a single, flexible framework that can express all these tasks, and train on heterogeneous datasets, should both improve generalization across 3D tasks and substantially reduce deployment overhead.

Our approach, OMNIVIEW, instantiates such a unified framework as a single video generative model for diverse view-synthesis tasks. We model each image  $\mathbf{I}$  as a sample from a 4D world, parameterized by a camera pose  $\mathbf{p}$  and a timestamp  $t$ . Under this view, static multi-view NVS corresponds to varying  $\mathbf{p}_{1:N}$  and a target pose  $\mathbf{p}^t$  while keeping  $t$  fixed; I2V with camera control corresponds to predicting frames at future times  $t_{1:N}$  along target poses  $\mathbf{p}_{1:N}^t$  given an input  $(\mathbf{I}_0, \mathbf{p}_0, t_0)$ ; and V2V camera redirection corresponds to re-rendering an input video from new poses  $\mathbf{p}_{1:N}^t$  at the same timestamps  $t_{1:N}$  as the source.

To realize this unified 4D formulation, we adopt a Diffusion Transformer (DiT) [49] backbone that naturally handles a variable number of input tokens. We tokenize each frame into a set of video tokens, concatenate tokens from all available inputs (images, views, or frames), and condition generation on this sequence. DiTs already support temporal reasoning via spatio-temporal Rotary Positional Embeddings (3D RoPE), which encode  $(x, y, t)$  for each token. Prior works typically injects camera information by either encoding poses with a pose encoder or by mapping them to Plücker ray embeddings and then applying 3D RoPE [53] to both video and camera-conditioned tokens. This entangles camera pose  $\mathbf{p}$  and time  $t$  in a single positional embedding space, making it difficult for the model to learn 3D structure independently of temporal dynamics and often leading to overfitting to seen trajectories.

In contrast, OMNIVIEW explicitly disentangles space and time. We represent each token’s camera only to as ase Plücker nd apply *spatial* 2D RoPE only to these Plucker features, then concatenate the them channel-wise with the

corresponding video token. Time is encoded separately via temporal RoPE on the video tokens. This design cleanly separates camera geometry from temporal evolution, while still allowing the DiT to jointly attend over all tokens. Combined with the corresponding video token. Time is encoded separately via temporal RoPE on the video tokens. This design cleanly separates camera geometry from temporal evolution, while still allowing the DiT to jointly attend over all tokens. Combined with the variable-token design, this lets OMNIVIEW flexibly ingest arbitrary combinations of frames, views, and timestamps and thereby support a wide range of 4D inputs, under a single architecture. We then the variable-token design, this lets OMNIVIEW flexibly ingest arbitrary combinations of frames, views, and timestamps and thereby support a wide range of 4D inputs under a single architecture. We then devise a joint training strategy that mixes heterogeneous 3D datasets, each correspondconditioned on text and images. OMNIVIEW, 3D-consistently matches or outperforms specialized baselines, producing to different task configurations (multi-view static, dynamic, T2V/I2V with camera control, V2V redirection), so that the model learns shared geometric priors across them.

We extensively evaluate OMNIVIEW on static and dynamic NVS benchmarks with monocular and multi-view inputs, as well as camera-control tasks conditioned on text and images. OMNIVIEW consistently matches or outperforms specialized baselines, producing high-fidelity, 3D-consistent videos and camera-conditioned tokens. With up to 33% increase in SSIM scores in multiview NVS LLFF dataset, 60% in dynamic NVS Neural 3D Video benchmark, 20% in static camera control on RE-10K, 4x reduction in camera errors in text-conditioned video generation, OMNIVIEW demonstrates strong 3D consistency and fidelity across tasks, and generalization to input configurations not seen during training. Ablations validate the benefit of our RoPE design.

## 2. Related Work

**Camera-Controllable Video Generation.** The emergence of powerful text-to-video diffusion models [9, 12, 17, 44, 80] has fueled extensive research on conditioning generated videos with additional controls, such as camera parameters [3, 20, 39, 52, 57, 67, 68, 79, 89, 90]. Early camera-control approaches integrate extrinsic camera information as part of the diffusion model’s conditioning, either through tailored encoders or numeric input channels. Models like MotionCtrl [67] and CameraCtrl [21] encode camera poses or trajectories to enable user-directed viewpoint changes throughout video generation, but often require specific paired training data and show limited generalization when camera motions deviate from training regimes. Other strategies bypass model retraining by employing 3D geo-

metric cues, for example warping frames using estimated depth to match new camera placements and feeding these as priors during the denoising process [23, 81], though these methods face a trade-off between enforcing geometric consistency and visual fidelity.

**Novel View Synthesis and Video-to-Video Generation.** Generating unseen viewpoints from posed images or videos has advanced significantly in recent years [6, 7, 16, 24, 29, 35, 42, 46, 47, 55, 66, 76, 86]. Conventional novel view synthesis (NVS) frameworks leverage volumetric or Gaussian-based scene representations; meanwhile, feed-forward architectures [10, 11, 14, 26, 50, 56, 63, 82, 92] aim to directly predict target views from sparse or multi-view input, but usually struggle in generalization tasks or under challenging domain shifts. Some recent works attempt to harness image/video generative models to infuse prior knowledge and regularize deficits of view synthesis, as in ReconFusion [70] and CAT3D [18]. However, these strategies tend to be slow due to per-scene optimization and often depend on robust inter-view alignment, as seen in ReconX [38] and ViewCrafter [85], which become error-prone in the presence of thin or ambiguous structures. Relatedly, the video-to-video generation field [13, 40, 43, 62, 64, 65, 75, 77, 93] explores producing temporally consistent and controllable video outputs under various manipulation and conditioning tasks. Techniques such as GCD [57], Recapture [87], GS-DiT [8], DAS [19], and recent 4D-consistent pipelines [51, 72, 83] exploit geometric and dynamic scene information, such as tracked 3D points [28, 71], to condition or align the generative models, either via simulation or real-world sequences. These approaches enable synchronizing generated outputs across multiple cameras or time but are typically constrained by how accurately dynamic scene content can be retrieved or tracked. Some works tackle 4D and multi-view video generation by training generative models directly on synchronized video collections [4, 31, 60, 61, 69, 73], or by reconstructing an explicit scene representation first and then rendering views [36, 38, 54, 88].

**Consistency in Video Generation.** Ensuring frame-to-frame and cross-view temporal or geometric consistency remains a critical challenge in video synthesis. Early efforts used 3D point clouds or height maps derived from input or generated content to guide learning and enforce consistency [15, 43]. Others [30] propagate consistency across parallel generated video streams but may lose coherence when scene elements leave the views of all sequences. Latent feature histories have also been used to improve consistency for streaming or autoregressive video generation approaches [22], though explicit, interpretable 3D control remains an open research direction.

### 3. Method

#### 3.1. Preliminary: Video Diffusion Models

Our framework builds on the popular architecture used in state-of-the-art text-to-video diffusion models [1, 17, 59, 80], which combine a 3D Variational Auto-Encoder (VAE) with a Diffusion Transformer (DiT) [49]. The VAE spatially and temporally compresses input videos into low-resolution latents that serve as compact representations for diffusion modeling. The diffusion process follows the rectified flow formulation [41], where the model learns to transform noise into coherent video latents through velocity prediction.

Within this framework, the DiT operates directly in latent space. It first patchifies the 3D latent tensor into spatio-temporal tokens  $\mathbf{z}_{xyt} \in \mathbb{R}^d$ , where  $x$ ,  $y$ , and  $t$  denote the spatial and temporal coordinates of each  $d$ -dimensional token. These tokens are then processed through a stack of transformer blocks, each comprising a 3D spatio-temporal self-attention layer to capture motion and appearance consistency, a text cross-attention layer for semantic conditioning, and a feed-forward network (FFN) for feature transformation. This architecture enables efficient large-scale training and produces high-quality, temporally consistent video generations.

In this work, we extend the capabilities of DiT-based diffusion architectures to support a wider range of camera control and multi-view synthesis tasks.

#### 3.2. Network architecture

As illustrated in Figure 2, the proposed model takes as input a set of images captured from different viewpoints and time steps, represented using Plücker ray maps. The objective is to denoise the target tokens to generate video frames at any user-specified viewpoint and time. The configurations of context and target viewpoints and timestamps are flexible, enabling the model to adapt to a wide range of tasks.

To realize this capability, we next investigate the optimal designs for integrating context-frame conditioning, camera control, and the corresponding training strategies that best support these functionalities.

**Context image conditioning.** To facilitate flexibility and scalability in the number of inputs to our model, we propose a network that performs token concatenation as inputs to the DiT. The network takes as input a set of context tokens  $\mathbf{z}_{xyt}^{\text{ctx}}$  (encoded from multiple input views), which are concatenated token-wise with a set of target tokens  $\mathbf{z}_{xyt}^{\text{tgt}}$ , where  $x$ ,  $y$ , and  $t$  denote the spatial and temporal coordinates of the token vector. During the flow matching process, the target tokens are progressively denoised, where  $x$ ,  $y$ , and  $t$  denote the spatial and temporal coordinates of the token vector. During the flow matching process, the target tokens are progressively denoised while attending to the clean context tokens, which serve as conditioning inputs to

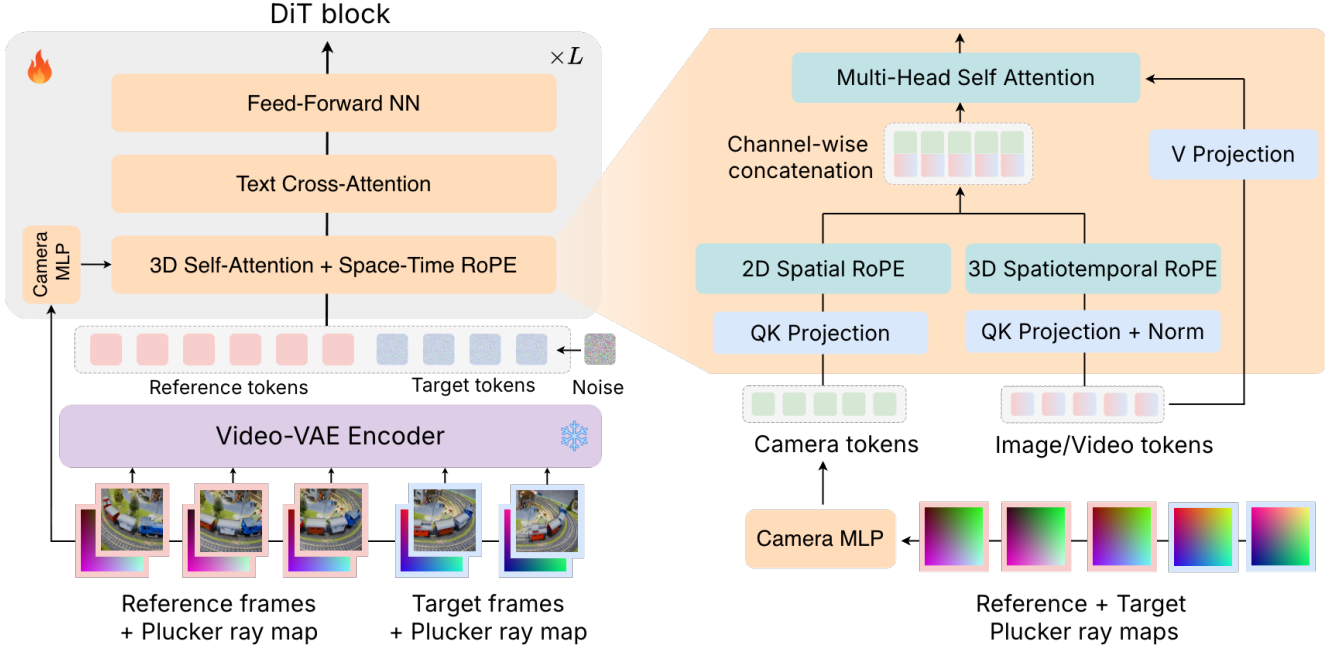


Figure 2. Overview of the network architecture. We concatenate source input tokens and partly denoised target tokens as input to the DiT. Right: We apply an MLP to the camera embeddings for each view followed by separate RoPE mechanisms for camera and video tokens. The two sets of tokens are channel-wise concatenated when input to the Self-Attention block.

guide generation. The overall input to the DiT is therefore represented as a joint sequence composed of both  $\mathbf{z}^{\text{ctx}}$  and  $\mathbf{z}^{\text{tgt}}$ .

**Camera embeddings.** To incorporate camera information, we utilize Plücker ray maps  $\mathbf{P} \in \mathbb{R}^{6 \times H \times W}$ , which represent the camera ray direction and origin for each image pixel. Our camera encoder  $\mathcal{E}_c$  divides the ray map into patch volumes with the same spatio-temporal compression rate as the video VAE + DiT patchifier. These patch volumes are flattened channel-wise and passed through an MLP to obtain a set of camera tokens for both context and target frames, denoted as  $\mathbf{c}_{xyt}^{\text{ctx}}$  and  $\mathbf{c}_{xyt}^{\text{tgt}}$ , with resolution and channels matching that of the video tokens. Separate camera encoders are employed for each DiT layer, allowing the model to flexibly modulate the influence of camera conditions at different stages of the network.

A naive strategy for injecting camera tokens  $\mathbf{c}_{xyt}$  is to simply concatenate or add them to the corresponding video tokens  $\mathbf{z}_{xyt}$ . A similar approach is adopted in [5], where a camera encoder produces a 12-dimensional pose embedding that is added to the video tokens in every DiT block. However, this formulation entangles the spatial location of the camera and the temporal position of the corresponding frame within the video, as discussed below.

**Disentangle camera and temporal position embeddings.** Video DiTs use 3D Rotary Positional Embeddings (RoPE) [53] to encode the spatial-temporal positions  $(x, y, t)$  of video tokens. Specifically, RoPE applies a

frequency-based rotation on the keys and values of a token:

$$\text{RoPE}(\mathbf{q}_{xyt}^z) = R(\mathbf{q}_{xyt}^z, \theta_{xyt}), \quad (1)$$

where  $\theta_{xyt}$  denotes the sinusoidal phase parameters set by the position  $(x, y, t)$ , see supplementary for details.  $\mathbf{q}_{xyt}^z$  denotes the query vector corresponding to the video tokens  $\mathbf{z}$ , and Eq. 1 is similarly applied to the key vectors  $\mathbf{k}_{xyt}^z$ .

When camera embeddings  $\mathbf{c}_{xyt}$  are directly added to the video tokens prior to applying 3D RoPE, the transformation becomes:

$$R(\mathbf{q}_{xyt}^z + \mathbf{c}_{xyt}^z, \theta_{xyt}) = R(\mathbf{q}_{xyt}^z, \theta_{xyt}) + R(\mathbf{c}_{xyt}^z, \theta_{xyt}), \quad (2)$$

since RoPE is a linear projection. This formulation, however, entangles camera and temporal information: the camera embeddings are rotated according to their specific camera corresponding timestamp  $t$ , even though they should ideally remain temporally invariant. Consequently, the model tends to overfit to the specific camera or unseen camera trajectories seen during training, as it implicitly encodes temporal correlations into the camera embeddings. This reduces generalization to novel or unseen camera trajectories, as further discussed in Sec. 4.4.

To address this issue and disentangle camera and temporal representations, we propose the following approach:

**(i) Setting  $t$  as a constant for camera tokens.** To eliminate the temporal interference on the camera tokens, we propose fixing their temporal index to a constant value, i.e.,  $t = 0$ ,

effectively reducing the 3D RoPE to a 2D form. Under this modification, separate RoPE transformations are applied to the video tokens and the camera tokens as follows:

$$\tilde{\mathbf{q}}_{xyt}^z = R(\mathbf{q}_{xyt}, \theta_{xyt}), \quad \tilde{\mathbf{c}}_{xyt} = R(\mathbf{c}_{xyt}, \theta_{xy0}). \quad (3)$$

For brevity, the corresponding formulation for the key vectors  $\tilde{\mathbf{k}}_{xyt}^z$  of the video tokens is omitted.

**(ii) Channel-wise concatenation of video and camera tokens.** The RoPE-transformed camera tokens  $\tilde{\mathbf{c}}$  and the video queries and keys  $\tilde{\mathbf{q}}^z$ ,  $\tilde{\mathbf{k}}^z$  must be fused before being fed into the scaled dot-product attention. This fusion can be performed either additively or via channel-wise concatenation. To analyze the design choices, we compare the resulting attention scores under both strategies.

Let  $m = (x, y, t)$  and  $n = (x', y', t')$  denote the spatial-temporal positions of the query and key tokens, respectively. Under additive fusion, the attention score is given by:

$$A_{n,m}^{\text{add}} = \langle \tilde{\mathbf{q}}_m^z + \tilde{\mathbf{c}}_m, \tilde{\mathbf{k}}_n^z + \tilde{\mathbf{c}}_n \rangle, \quad (4)$$

where  $\langle \cdot, \cdot \rangle$  denotes the inner product. We observe that  $A_{n,m}^{\text{add}}$  introduces entangled cross-terms between the camera and temporal positions, *i.e.*  $\langle \tilde{\mathbf{q}}_m^z, \tilde{\mathbf{c}}_n \rangle$  and  $\langle \tilde{\mathbf{k}}_n^z, \tilde{\mathbf{c}}_m \rangle$ , which can lead to undesirable deviations in the attention map and unstable interactions between spatial-temporal and camera embeddings.

Instead, we advocate for *channel-wise concatenation* of the video and camera tokens, yielding an attention score of:

$$A_{n,m}^{\text{cat}} = \langle [\tilde{\mathbf{q}}_m^z; \tilde{\mathbf{c}}_m], [\tilde{\mathbf{k}}_n^z; \tilde{\mathbf{c}}_n] \rangle = \langle \tilde{\mathbf{q}}_m^z, \tilde{\mathbf{k}}_n^z \rangle + \langle \tilde{\mathbf{c}}_m, \tilde{\mathbf{c}}_n \rangle, \quad (5)$$

where the camera tokens and video tokens are fully disentangled. In the canonical case where two frames share the same camera configuration, regardless of their temporal index, the concatenation formulation yields a constant offset in the attention map, thereby maintaining behavior closely aligned with the original temporal attention structure, as desired. We show ablations by exploring the two RoPE variants in Table 6 supporting our hypothesis.

**(iii) Separate QK projections for camera tokens.** Finally, we find it crucial to further enhance the representation capacity of camera tokens by introducing independent query and key (QK) projection layers that transform the camera embeddings  $\mathbf{c}$  into  $\mathbf{q}^c$  and  $\mathbf{k}^c$ . This modification allows the model to learn camera-specific attention patterns distinct from those of the video tokens.

The resulting transformer architecture, illustrated in Fig. 2, computes the attention score as:

$$A_{n,m}^{\text{cat}} = \langle \tilde{\mathbf{q}}_m^z, \tilde{\mathbf{k}}_n^z \rangle + \langle \tilde{\mathbf{q}}_m^c, \tilde{\mathbf{k}}_n^c \rangle, \quad (6)$$

where  $\tilde{\mathbf{q}}_m^c$ ,  $\tilde{\mathbf{k}}_n^c$  denote the 2D RoPE-transformed query and key vectors for the camera tokens.

Table 1. Multitask training configurations for various datasets in terms of number of views  $V$  and number of latent frames  $F$ .

| Task Type  | Datasets                     | Context<br>( $V \times F$ ) | Target<br>( $V \times F$ )                    |
|--|------------------------------|-----------------------------|---|
| Monocular<br>Image NVS,<br>Multi-view<br>Image NVS | RE10K,<br>DL3DV,             | $3 \times 1$                |   |
|  | ReCamMaster,                 | $2 \times 1$                | $1 \times 1$                                  |
|  | SynCamMaster                 | $1 \times 1$                |   |
| Monocular<br>Video NVS                             | ReCamMaster,                 | $1 \times 3$                | $1 \times 3$                                  |
|  | SynCamMaster                 |                             |   |
|  | RE10K,<br>DL3DV,<br>Stereo4D | -                           | $1 \times 3$<br>$1 \times 5$<br>$1 \times 10$ |
| T2V + CamCtrl<br>I2V + CamCtrl                     | RE10K,<br>DL3DV,             | $1 \times 1$                | $1 \times 3$<br>$1 \times 5$                  |
|  | Stereo4D                     |                             | $1 \times 10$                                 |
|  | RE10K,<br>DL3DV,             |                             |   |
| V2V + CamCtrl                                      | Stereo4D                     |                             |   |
|  | RE10K,<br>DL3DV,             | $1 \times 3$                | $1 \times 3$<br>$1 \times 5$                  |
|  | Stereo4D                     |                             | $1 \times 10$                                 |

### 3.3. Training setup

To enable the model to accommodate different input configurations across a variety of tasks, we leverage a diverse collection of existing 3D/4D datasets encompassing multiple data types. Stereo4D [27] comprises stereo videos with camera-pose annotations; however, because per-video stereo baselines are unavailable, we use a single view with its corresponding pose, effectively treating it as a monocular video dataset. We include RE10K [94] and DL3DV [37] as multi-view image NVS datasets. For image/video NVS, we additionally use the synthetic Syncamaster [4] and Recammaster [5] datasets, featuring multiple time-synchronized static cameras and dynamic camera trajectories, respectively. An overview of the datasets and the tasks each dataset supports is provided in Tab. 1. We primarily target context and target configurations with 1, 3, 5, or 10 latent frames, and up to 3 views for the context input. Owing to the variation in input views and frames across training iterations, we demonstrate in Fig. 5 that our model generalizes to longer video sequences and a greater number of views. Moreover, despite not training directly on the multi-view video NVS task (*e.g.*,  $3 \times 3 \rightarrow 1 \times 3$ ), the model generalizes to it naturally, as it can be viewed as a composition of the multi-view image NVS and monocular video NVS tasks.

During training, we randomly sample a task and then select a dataset that supports it. Static and dynamic NVS tasks sample identical timestamps for context and target frames. In contrast, for camera-control (CamCtrl) tasks, we sample target frames such that the first target index  $t_0^{\text{tgt}}$  lies within

a temporal offset  $\Delta$  (a task-dependent hyperparameter) of the first context index  $t_0^{\text{ctx}}$ , *i.e.*,  $|t_0^{\text{gt}} - t_0^{\text{ctx}}| \leq \Delta$ . This enables I2V and V2V not only for consecutive future timestamps relative to the inputs but also for earlier frames where the context precedes the target, thereby enhancing temporal versatility with last-frame/middle-frame image conditioning.

## 4. Experiments

The key takeaways of our experiments are: a) OMNIVIEW is capable of high quality 4D consistency tasks across a wide variety of settings, including camera control and novel view synthesis for both static and dynamic scenes. b) Compared to specialized methods that focuses on specific settings, OMNIVIEW effectively combines many types of camera and time conditions via our proposed RoPE, leading to generalization across a variety of tasks. c) As the number of input views increase, OMNIVIEW is able to effectively leverage the increased signal in the input to improve reconstruction quality. d) Through ablations, we show that our proposed camera RoPE design is crucial for effective modeling of camera and time conditions, leading to improved performance across tasks.

### 4.1. Experimental Setup

**Implementation Details.** As discussed in Sec. 3.3, we train OMNIVIEW on a mixture of the datasets provided in Tab. 1. We choose the Wan 2.1 1.1B model [59] as the base architecture for all our experiments unless mentioned otherwise. Each iteration takes in a set of source views, target views and their corresponding cameras as well as their timestamps in the real world. We train the model for 40K iterations over 32 H100 GPUs. We linearly warmup the learning rate for 3K iterations upto 0.0001 with a batch size of 64. During the warmup stage, we exclusively train on the multiview static task to quickly update the parameters corresponding to the Plucker ray maps while also allowing the model to quickly adapt to camera conditioning.

**Evaluation and Baselines.** We comprehensively evaluate OMNIVIEW on a wide variety of 3D/4D tasks. We broadly group multiple tasks under: a) Monocular Video NVS (Tab. 2) b) Multi-view Image and Video NVS (Tab. 3) and c) T2V/I2V + Camera Control. We mainly perform comparisons with closely related generative view-synthesis works of RecamMaster [5], TrajectoryCrafter [83], and GEN3C [51] on the Monocular Video NVS as well as the I2V + Camera Control task. For Multi-view Image NVS, GEN3C and SEVA [91] are our primary baselines which can take multiple view inputs. We visualize the results from our model in Fig. 3 and comparisons in the supplementary. We use the reconstruction metrics of PSNR, SSIM, LPIPS for datasets with GT views available. We additionally evaluate the quality of the camera trajectory via Ro-

tation (RotErr) and Translation Error (TrErr) as proposed by [21]. We use MegaSaM [36] for estimating camera trajectories from generated videos when comparing with the GT trajectories. We additionally compute the metric scale for each scene similar to [2] and scale the camera translation vectors accordingly. We find this necessary for monocular view cases which have inherent scale ambiguity.

### 4.2. Monocular Video NVS

For this task, we extract camera trajectories for 45 real-world videos from DAVIS [25]. For each video, we use 4 predefined trajectory paths from RecamMaster evaluations and 1 new trajectory which is a spiral path. Results are summarized in Tab. 2. Averaged over all trajectories, we match the performance of SOTA approaches of [5, 51, 83] in terms of camera error metrics despite being trained on a large diversity of tasks. We additionally visualize qualitative results in the supplementary. We see that we obtain high fidelity generations compared to other works with fewer motion artifacts. We maintain high temporal synchronization compared to the input condition highlighting the capability of the model to accurately extract appearance information from conditioning views while disentangling camera and time conditions.

Beyond camera trajectory error metrics, we also compare with [51, 83] on the Neural 3D Video (N3DV) dataset [33] which consists of multi-view static cameras capturing a dynamic scene. We choose the first view as the test and choose one training view with significant disparity from the test. Compared to prior works, we obtain high quality reconstructions which are well aligned with the GT achieving better PSNR, SSIM and LPIPS. Note that our conditioning is largely implicit via encoded latents and we do not use any form of explicit 3D supervision such as depth or point clouds apart from the metric scene scale. Despite being trained on 122K camera trajectories, RecamMaster fails for this setting of static target camera and tends to implicitly induce camera motion. This highlights the generalizability issue of using 3D spatiotemporal RoPE on camera conditions as discussed in Sec. 3 where the model fails to disentangle camera and time resulting in poor out-of-distribution trajectory performance.

#### 4.2.1. Multi-view Static and Dynamic NVS

We now extend our approach to the multi-view input setting consisting of images or time-synchronized videos. We first evaluate OMNIVIEW on the LLFF dataset [45] consisting of multiple view captures of a static scene. We sparsely sample 3, 6, or 9 input views and choose one test view. We compare against SEVA [91] and GEN3C as they allow for multiple view inputs. Results are summarized in Tab. 3, measuring the 3 reconstruction metrics. We see that we perform competitively against the baselines across 3 metrics. While GEN3C is limited by its cache size which is 4 by



**Figure 3. Example generations from OMNIVIEW.** We show results on (a) dynamic NVS; (b) static NVS; (c) text-to-video (T2V) with camera control; and (d) image-to-video (I2V) with camera control. In all cases, OMNIVIEW produces high-fidelity, 3D-consistent videos that adhere to the input conditioning(s).

default, we directly generalize to more input views despite being trained on upto 3 static views, while improving reconstruction quality with additional 3D information of the scene.

This is observed in the dynamic setting as well for N3DV, where we continue to improve reconstruction quality from 1 to 5 views Fig. 5 in terms of PSNR, SSIM, and LPIPS. We visualize the reconstructions in Fig. 4. As the

Table 2. Quantitative comparison on different camera trajectory types on DAVIS. We perform competitively against prior SOTA Video NVS approaches while outperforming in certain categories.

| Method                 | Trans Up           |                     | Trans Down         |                     | Arc Left           |                     | Arc Right          |                     | Spiral w/ Zoom     |                     | Overall            |                     |
|------------------------|--------------------|---------------------|--------------------|---------------------|--------------------|---------------------|--------------------|---------------------|--------------------|---------------------|--------------------|---------------------|
|                        | TrErr $\downarrow$ | RotErr $\downarrow$ |
| TrajectoryCrafter [84] | 24.77              | 3.59                | 21.36              | 3.60                | 14.37              | 4.00                | 24.92              | 2.64                | 23.11              | 2.05                | 21.70              | 3.18                |
| ReCamMaster [5]        | <b>10.18</b>       | 2.60                | <b>11.47</b>       | <b>2.19</b>         | <b>8.85</b>        | 3.39                | <b>16.49</b>       | 2.82                | <b>13.49</b>       | 2.37                | <b>12.09</b>       | 2.67                |
| Gen3C [51]             | 28.38              | <b>1.88</b>         | 42.55              | <b>2.04</b>         | 129.17             | <b>2.62</b>         | 21.80              | <b>1.39</b>         | 25.72              | <b>1.71</b>         | 49.52              | <b>1.93</b>         |
| <b>OMNIVIEW</b>        | <u>11.75</u>       | <u>2.20</u>         | <u>20.51</u>       | 2.46                | <b>5.77</b>        | <u>3.27</u>         | <b>8.88</b>        | <u>2.50</u>         | <u>14.53</u>       | <u>2.03</u>         | <u>12.29</u>       | <u>2.49</u>         |

Table 3. Quantitative comparison on LLFF dataset. We outperform Stable Virtual Camera [91] significantly in terms of reconstruction quality for the static NVS task.

| Method          | Views | PSNR $\uparrow$ | SSIM $\uparrow$ | LPIPS $\downarrow$ |
|-----------------|-------|-----------------|-----------------|--------------------|
| SEVA [91]       | 3     | 14.84           | 0.30            | 0.46               |
| <b>OMNIVIEW</b> |       | <b>15.43</b>    | <b>0.38</b>     | <b>0.41</b>        |
| SEVA [91]       | 6     | 15.36           | 0.32            | 0.43               |
| <b>OMNIVIEW</b> |       | <b>16.11</b>    | <b>0.42</b>     | <b>0.38</b>        |
| SEVA [91]       | 9     | 15.60           | 0.33            | 0.42               |
| <b>OMNIVIEW</b> |       | <b>16.49</b>    | <b>0.45</b>     | <b>0.34</b>        |

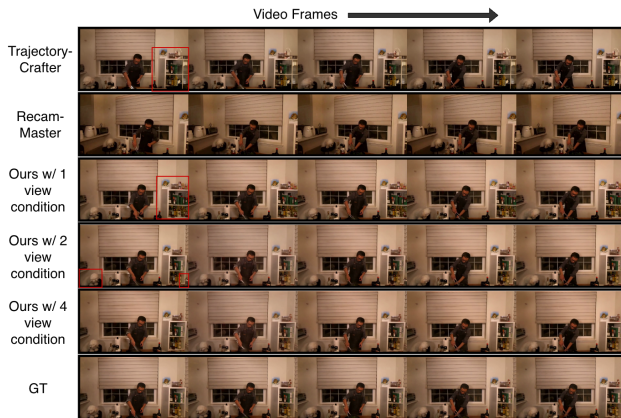


Figure 4. Qualitative visualizations on a scene in the N3DV dataset. We consistently outperform [5, 83] on single view input while improving reconstruction quality with increasing number of input conditions.

number of views increase, the model is able to better resolve the scale ambiguity with static cameras producing increasingly more aligned generations with the GT view.

Notably, our training configuration (Tab. 1) does not include the multi-view dynamic NVS task but only on multi-view static NVS and monocular dynamic NVS. This highlights the capability of our model to generalize to not only more views or more frames, but also to new 3D/4D tasks

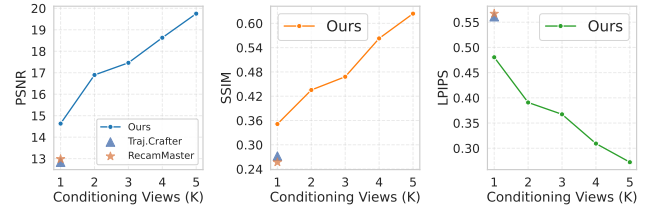


Figure 5. Increasing number of conditional views improves reconstruction on N3DV [33] and is more aligned with the GT.

Table 4. Quantitative comparison on RE10K dataset. We continue to outperform [51, 83] on the Image-to-Video + Camera Control task across all reconstruction metrics.

| Method                 | PSNR $\uparrow$ | SSIM $\uparrow$ | LPIPS $\downarrow$ |
|------------------------|-----------------|-----------------|--------------------|
| TrajectoryCrafter [84] | 16.94           | 0.53            | 0.36               |
| Gen3C [51]             | 17.34           | 0.55            | 0.34               |
| <b>OMNIVIEW</b>        | <b>19.20</b>    | <b>0.66</b>     | <b>0.28</b>        |

Table 5. Camera-error metrics on RE-10K for the T2V+Camera Control task. We outperform AC3D across both metrics.

| Metric                | AC3D [2] | OMNIVIEW     |
|-----------------------|----------|--------------|
| TransErr $\downarrow$ | 5.170    | <b>1.412</b> |
| RotErr $\downarrow$   | 1.365    | <b>0.572</b> |

which are combinations of trained tasks. This opens the avenue to potentially include a variety of inputs such as multiple view combinations of images and videos.

### 4.3. T2V/I2V + Camera Control

While NVS targets generations with timestamps which are same as input conditions, T2V/I2V + Camera Control involves target timestamps which are in the future from the image condition for I2V. Additionally, we show that the model also generalizes to T2V by passing no conditional views but only specifying target trajectories. We evaluate both T2V/I2V on RE10K on a subset of 1000/2000 sam-

Table 6. Ablation study exploring different RoPE variants.

| Variant                    | PSNR↑        | SSIM↑        | LPIPS↓       |
|----------------------------|--------------|--------------|--------------|
| No RoPE applied to Plucker | 13.36        | 0.292        | 0.554        |
| Apply 3D RoPE to Plucker   | 13.68        | 0.309        | 0.509        |
| Apply 2D RoPE to Plucker   | 14.17        | 0.345        | 0.504        |
| + Plucker to values        | 14.25        | 0.334        | 0.524        |
| <b>Ours: + Attn Cat</b>    | <b>15.46</b> | <b>0.376</b> | <b>0.456</b> |

ples respectively. We compare with TrajectoryCrafter and Gen3C on I2V, and with AC3D on T2V. Results are summarized in Tabs. 4 and 5.

We see that we obtain better reconstructions aligned with the GT views compared to [51, 83] while also more closely aligning with the camera trajectory compared to AC3D [2]. This is despite AC3D being trained primarily on the Camera Control task while we train on a variety of different 3D/4D tasks. Qualitative results are provided in the supplementary to show high video fidelity obtained even in the case of no input conditioning views.

#### 4.4. Ablation Study: Camera RoPE

We conduct an ablation study to analyze the contribution of different components in our camera RoPE approach. Table 6 shows the performance of various configurations on the N3DV dataset.

Our final approach with attention head concatenation achieves the best performance across all metrics, demonstrating the effectiveness of our design choices.

### 5. Conclusion

In this work, we introduced OMNIVIEW, a novel framework for 4D consistent video generation that effectively integrates camera and time conditions using our camera RoPE. Our approach demonstrates superior performance across various tasks, including camera control and novel view synthesis for both static and dynamic scenes. Through extensive experiments and ablation studies, we validated the effectiveness of our design choices, particularly the use of RoPE for modeling camera and time conditions. Future work could explore further enhancements to the model architecture and investigate additional applications in 4D content generation.

### References

- [1] Niket Agarwal, Arslan Ali, Maciej Bala, Yogesh Balaji, Erik Barker, Tiffany Cai, Prithvijit Chattopadhyay, Yongxin Chen, Yin Cui, Yifan Ding, et al. Cosmos world foundation model platform for physical ai. *arXiv preprint arXiv:2501.03575*, 2025. 3
- [2] Sherwin Bahmani, Ivan Skorokhodov, Guocheng Qian, Aliaksandr Siarohin, Willi Menapace, Andrea Tagliasacchi, David B Lindell, and Sergey Tulyakov. Ac3d: Analyzing and improving 3d camera control in video diffusion transformers. *arXiv preprint arXiv:2411.18673*, 2024. 6, 8, 9, 3, 4
- [3] Sherwin Bahmani, Ivan Skorokhodov, Aliaksandr Siarohin, Willi Menapace, Guocheng Qian, Michael Vasilkovsky, Hsin-Ying Lee, Chaoyang Wang, Jiaxu Zou, Andrea Tagliasacchi, et al. Vd3d: Taming large video diffusion transformers for 3d camera control. *arXiv preprint arXiv:2407.12781*, 2024. 2
- [4] Jianhong Bai, Menghan Xia, Xintao Wang, Ziyang Yuan, Xiao Fu, Zuozhu Liu, Haoji Hu, Pengfei Wan, and Di Zhang. Syncammaster: Synchronizing multi-camera video generation from diverse viewpoints. *arXiv preprint arXiv:2412.07760*, 2024. 1, 3, 5
- [5] Jianhong Bai, Menghan Xia, Xiao Fu, Xintao Wang, Lianrui Mu, Jinwen Cao, Zuozhu Liu, Haoji Hu, Xiang Bai, Pengfei Wan, and Di Zhang. Recammaster: Camera-controlled generative rendering from a single video, 2025. 1, 2, 4, 5, 6, 8
- [6] Jonathan T. Barron, Ben Mildenhall, Matthew Tancik, Peter Hedman, Ricardo Martin-Brualla, and Pratul P. Srinivasan. Mip-NeRF: a multiscale representation for anti-aliasing neural radiance fields. *ICCV*, 2021. 3
- [7] Jonathan T. Barron, Ben Mildenhall, Dor Verbin, Pratul P. Srinivasan, and Peter Hedman. Mip-NeRF 360: unbounded anti-aliased neural radiance fields. *CVPR*, 2022. 3
- [8] Weikang Bian, Zhaoyang Huang, Xiaoyu Shi, Yijin Li, Fu-Yun Wang, and Hongsheng Li. Gs-dit: Advancing video generation with pseudo 4d gaussian fields through efficient dense 3d point tracking. *arXiv preprint arXiv:2501.02690*, 2025. 3
- [9] Andreas Blattmann, Tim Dockhorn, Sumith Kulal, Daniel Mendelevitch, Maciej Kilian, Dominik Lorenz, Yam Levi, Zion English, Vikram Voleti, Adam Letts, et al. Stable video diffusion: Scaling latent video diffusion models to large datasets. *arXiv preprint arXiv:2311.15127*, 2023. 2
- [10] David Charatan, Sizhe Lester Li, Andrea Tagliasacchi, and Vincent Sitzmann. PixelSplat: 3D Gaussian splats from image pairs for scalable generalizable 3D reconstruction. In *CVPR*, 2024. 3
- [11] Anpei Chen, Zexiang Xu, Fuqiang Zhao, Xiaoshuai Zhang, Fanbo Xiang, Jingyi Yu, and Hao Su. MVSNeRF: fast generalizable radiance field reconstruction from multi-view stereo. In *ICCV*, pages 14124–14133, 2021. 3
- [12] Haoxin Chen, Yong Zhang, Xiaodong Cun, Menghan Xia, Xintao Wang, Chao Weng, and Ying Shan. Videocrafter2: Overcoming data limitations for high-quality video diffusion models. In *Proceedings of the IEEE/CVF Conference*

on Computer Vision and Pattern Recognition, pages 7310–7320, 2024. 2

[13] Qihua Chen, Yue Ma, Hongfa Wang, Junkun Yuan, Wenzhe Zhao, Qi Tian, Hongmei Wang, Shaobo Min, Qifeng Chen, and Wei Liu. Follow-your-canvas: Higher-resolution video outpainting with extensive content generation. *arXiv preprint arXiv:2409.01055*, 2024. 3

[14] Yuedong Chen, Haofei Xu, Chuanxia Zheng, Bohan Zhuang, Marc Pollefeys, Andreas Geiger, Tat-Jen Cham, and Jianfei Cai. MVSplat: efficient 3D Gaussian splatting from sparse multi-view images. In *ECCV*, 2024. 3

[15] Boyang Deng, Richard Tucker, Zhengqi Li, Leonidas Guibas, Noah Snavely, and Gordon Wetzstein. Streetscapes: Large-scale consistent street view generation using autoregressive video diffusion. In *ACM SIGGRAPH 2024 Conference Papers*, pages 1–11, 2024. 3

[16] Yuanxing Duan, Fangyin Wei, Qiyu Dai, Yuhang He, Wenzheng Chen, and Baoquan Chen. 4D-rotor Gaussian splatting: Towards efficient novel view synthesis for dynamic scenes. In *Proc. SIGGRAPH*, 2024. 3

[17] Weijie Kong et. al. Hunyuanyvideo: A systematic framework for large video generative models, 2024. 2, 3

[18] Ruiqi Gao, Aleksander Holynski, Philipp Henzler, Arthur Brussee, Ricardo Martin-Brualla, Pratul Srinivasan, Jonathan T. Barron, and Ben Poole. CAT3D: create anything in 3D with multi-view diffusion models. *arXiv preprint arXiv:2405.10314*, 2024. 1, 3

[19] Zekai Gu, Rui Yan, Jiahao Lu, Peng Li, Zhiyang Dou, Chenyang Si, Zhen Dong, Qifeng Liu, Cheng Lin, Ziwei Liu, et al. Diffusion as shader: 3d-aware video diffusion for versatile video generation control. *arXiv preprint arXiv:2501.03847*, 2025. 3

[20] Yuwei Guo, Ceyuan Yang, Anyi Rao, Zhengyang Liang, Yaohui Wang, Yu Qiao, Maneesh Agrawala, Dahua Lin, and Bo Dai. Animatediff: Animate your personalized text-to-image diffusion models without specific tuning. *arXiv preprint arXiv:2307.04725*, 2023. 2

[21] Hao He, Yinghao Xu, Yuwei Guo, Gordon Wetzstein, Bo Dai, Hongsheng Li, and Ceyuan Yang. Cameractrl: Enabling camera control for text-to-video generation. *arXiv preprint arXiv:2404.02101*, 2024. 1, 2, 6

[22] Roberto Henschel, Levon Khachatryan, Daniil Hayrapetyan, Hayk Poghosyan, Vahram Tadevosyan, Zhangyang Wang, Shant Navasardyan, and Humphrey Shi. Streaming2v: Consistent, dynamic, and extendable long video generation from text. *arXiv preprint arXiv:2403.14773*, 2024. 3

[23] Chen Hou, Guoqiang Wei, Yan Zeng, and Zhibo Chen. Training-free camera control for video generation. *arXiv preprint arXiv:2406.10126*, 2024. 3

[24] Binbin Huang, Zehao Yu, Anpei Chen, Andreas Geiger, and Shenghua Gao. 2D Gaussian splatting for geometrically accurate radiance fields. In *SIGGRAPH 2024 Conference Papers*. ACM, 2024. 3

[25] Jia-Bin Huang, Sing Bing Kang, Narendra Ahuja, and Jo-hannes Kopf. Temporally coherent completion of dynamic video. In *ACM*, 2016. 6

[26] Haian Jin, Hanwen Jiang, Hao Tan, Kai Zhang, Sai Bi, Tianyuan Zhang, Fujun Luan, Noah Snavely, and Zexiang Xu. LVSM: a large view synthesis model with minimal 3D inductive bias, 2024. 3

[27] Linyi Jin, Richard Tucker, Zhengqi Li, David Fouhey, Noah Snavely, and Aleksander Holynski. Stereo4D: Learning How Things Move in 3D from Internet Stereo Videos. In *Proceedings of the IEEE/CVF Conference on Computer Vision and Pattern Recognition*, 2025. 5

[28] Nikita Karaev, Ignacio Rocco, Benjamin Graham, Natalia Neverova, Andrea Vedaldi, and Christian Rupprecht. Co-tracker: It is better to track together. In *European Conference on Computer Vision*, pages 18–35. Springer, 2024. 3

[29] Bernhard Kerbl, Georgios Kopanas, Thomas Leimkühler, and George Drettakis. 3D Gaussian splatting for real-time radiance field rendering. *ACM Transactions on Graphics*, 42(4), 2023. 3

[30] Zhengfei Kuang, Shengqu Cai, Hao He, Yinghao Xu, Hongsheng Li, Leonidas Guibas, and Gordon Wetzstein. Collaborative video diffusion: Consistent multi-video generation with camera control. *arXiv preprint arXiv:2405.17414*, 2024. 3

[31] Bing Li, Cheng Zheng, Wenxuan Zhu, Jinjie Mai, Biao Zhang, Peter Wonka, and Bernard Ghanem. Vivid-zoo: Multi-view video generation with diffusion model. *Advances in Neural Information Processing Systems*, 37:62189–62222, 2024. 3

[32] Ruilong Li, Brent Yi, Junchen Liu, Hang Gao, Yi Ma, and Angjoo Kanazawa. Cameras as relative positional encoding, 2025. 1

[33] Tianye Li, Mira Slavcheva, Michael Zollhoefer, Simon Green, Christoph Lassner, Changil Kim, Tanner Schmidt, Steven Lovegrove, Michael Goesele, Richard Newcombe, et al. Neural 3d video synthesis from multi-view video. In *Proceedings of the IEEE/CVF conference on computer vision and pattern recognition*, pages 5521–5531, 2022. 6, 8

[34] Xinyang Li, Zhangyu Lai, Lining Xu, Yansong Qu, Liujuan Cao, Shengchuan Zhang, Bo Dai, and Rongrong Ji. Director3d: Real-world camera trajectory and 3d scene generation from text. *arXiv:2406.17601*, 2024. 1

[35] Zhaoshuo Li, Thomas Müller, Alex Evans, Russell H. Taylor, Mathias Unberath, Ming-Yu Liu, and Chen-Hsuan Lin. Neuralangelo: High-fidelity neural surface reconstruction. In *Proceedings of the IEEE/CVF Conference on Computer Vision and Pattern Recognition (CVPR)*, pages 8456–8465, 2023. 3

[36] Zhengqi Li, Richard Tucker, Forrester Cole, Qianqian Wang, Linyi Jin, Vickie Ye, Angjoo Kanazawa, Aleksander Holynski, and Noah Snavely. Megasam: Accurate, fast, and robust structure and motion from casual dynamic videos. *arXiv preprint arXiv:2412.04463*, 2024. 3, 6

[37] Lu Ling, Yichen Sheng, Zhi Tu, Wentian Zhao, Cheng Xin, Kun Wan, Lantao Yu, Qianyu Guo, Zixun Yu, Yawen Lu, et al. DL3DV-10K: a large-scale scene dataset for deep learning-based 3D vision. In *Proceedings of the IEEE/CVF Conference on Computer Vision and Pattern Recognition*, pages 22160–22169, 2024. 5

[38] Fangfu Liu, Wenqiang Sun, Hanyang Wang, Yikai Wang, Haowen Sun, Junliang Ye, Jun Zhang, and Yueqi Duan. Re-

conX: reconstruct any scene from sparse views with video diffusion model. *arXiv preprint arXiv:2408.16767*, 2024. 3

[39] Ruoshi Liu, Rundi Wu, Basile Van Hoorick, Pavel Tokmakov, Sergey Zakharov, and Carl Vondrick. Zero-1-to-3: Zero-shot one image to 3d object, 2023. 2

[40] Shaoteng Liu, Yuechen Zhang, Wenbo Li, Zhe Lin, and Jiaya Jia. Video-p2p: Video editing with cross-attention control. In *Proceedings of the IEEE/CVF Conference on Computer Vision and Pattern Recognition*, pages 8599–8608, 2024. 3

[41] Xingchao Liu, Chengyue Gong, and Qiang Liu. Flow straight and fast: Learning to generate and transfer data with rectified flow. *arXiv preprint arXiv:2209.03003*, 2022. 3

[42] Jonathon Luiten, Georgios Kopanas, Bastian Leibe, and Deva Ramanan. Dynamic 3D Gaussians: tracking by persistent dynamic view synthesis. In *3DV*, 2024. 3

[43] Arun Mallya, Ting-Chun Wang, Karan Sapra, and Ming-Yu Liu. World-consistent video-to-video synthesis. In *Proceedings of the European Conference on Computer Vision*, 2020. 3

[44] Willi Menapace, Aliaksandr Siarohin, Ivan Skorokhodov, Ekaterina Deyneka, Tsai-Shien Chen, Anil Kag, Yuwei Fang, Aleksei Stoliar, Elisa Ricci, Jian Ren, et al. Snap video: Scaled spatiotemporal transformers for text-to-video synthesis. In *Proceedings of the IEEE/CVF Conference on Computer Vision and Pattern Recognition*, pages 7038–7048, 2024. 1, 2

[45] Ben Mildenhall, Pratul P Srinivasan, Rodrigo Ortiz-Cayon, Nima Khademi Kalantari, Ravi Ramamoorthi, Ren Ng, and Abhishek Kar. Local light field fusion: Practical view synthesis with prescriptive sampling guidelines. *ACM Transactions on Graphics (ToG)*, 38(4):1–14, 2019. 6

[46] Ben Mildenhall, Pratul P. Srinivasan, Matthew Tancik, Jonathan T. Barron, Ravi Ramamoorthi, and Ren Ng. NeRF: representing scenes as neural radiance fields for view synthesis. *Communications of the ACM*, 65(1):99–106, 2021. 3

[47] Thomas Müller, Alex Evans, Christoph Schied, and Alexander Keller. Instant neural graphics primitives with a multiresolution hash encoding. *ACM Trans. Graph.*, 41(4):102:1–102:15, 2022. 3

[48] Jack Parker-Holder and Shlomi Fruchter. Genie 3: A new frontier for world models. Blog post, Google DeepMind, 2025. Accessed: YYYY-MM-DD. 1

[49] William Peebles and Saining Xie. Scalable diffusion models with transformers. In *Proceedings of the IEEE/CVF International Conference on Computer Vision*, pages 4195–4205, 2023. 2, 3

[50] Xuanchi Ren, Yifan Lu, Hanxue Liang, Zhangjie Wu, Huan Ling, Mike Chen, Sanja Fidler, Francis Williams, and Jiahui Huang. Scube: Instant large-scale scene reconstruction using voxsplats. *arXiv preprint arXiv:2410.20030*, 2024. 3

[51] Xuanchi Ren, Tianchang Shen, Jiahui Huang, Huan Ling, Yifan Lu, Merlin Nimier-David, Thomas Müller, Alexander Keller, Sanja Fidler, and Jun Gao. Gen3c: 3d-informed world-consistent video generation with precise camera control. In *Proceedings of the IEEE/CVF Conference on Computer Vision and Pattern Recognition*, 2025. 2, 3, 6, 8, 9

[52] Ruoxi Shi, Hansheng Chen, Zhuoyang Zhang, Minghua Liu, Chao Xu, Xinyue Wei, Linghao Chen, Chong Zeng, and Hao Su. Zero123++: a single image to consistent multi-view diffusion base model, 2023. 2

[53] Jianlin Su, Murtadha Ahmed, Yu Lu, Shengfeng Pan, Wen Bo, and Yunfeng Liu. Roformer: Enhanced transformer with rotary position embedding. *Neurocomputing*, 568:127063, 2024. 2, 4, 1

[54] Wenqiang Sun, Shuo Chen, Fangfu Liu, Zilong Chen, Yueqi Duan, Jun Zhang, and Yikai Wang. Dimensionx: Create any 3d and 4d scenes from a single image with controllable video diffusion. *arXiv preprint arXiv:2411.04928*, 2024. 3

[55] Matthew Tancik, Ethan Weber, Evonne Ng, Ruilong Li, Brent Yi, Justin Kerr, Terrance Wang, Alexander Kristoffersen, Jake Austin, Kamyar Salahi, Abhik Ahuja, David McAllister, and Angjoo Kanazawa. Nerfstudio: A modular framework for neural radiance field development. In *ACM SIGGRAPH 2023 Conference Proceedings*, 2023. 3

[56] Jiaxiang Tang, Zhaoxi Chen, Xiaokang Chen, Tengfei Wang, Gang Zeng, and Ziwei Liu. Lgm: Large multi-view gaussian model for high-resolution 3d content creation. *arXiv preprint arXiv:2402.05054*, 2024. 3

[57] Basile Van Hoorick, Rundi Wu, Ege Ozguroglu, Kyle Sargent, Ruoshi Liu, Pavel Tokmakov, Achal Dave, Changxi Zheng, and Carl Vondrick. Generative camera dolly: Extreme monocular dynamic novel view synthesis. *European Conference on Computer Vision (ECCV)*, 2024. 2, 3

[58] Vikram Voleti, Chun-Han Yao, Mark Boss, Adam Letts, David Pankratz, Dmitry Tochilkin, Christian Laforte, Robin Rombach, and Varun Jampani. Sv3d: Novel multi-view synthesis and 3d generation from a single image using latent video diffusion. In *European Conference on Computer Vision*, pages 439–457. Springer, 2024. 1

[59] Team Wan, Ang Wang, Baole Ai, Bin Wen, Chaojie Mao, Chen-Wei Xie, Di Chen, Feiwei Yu, Haiming Zhao, Jianxiao Yang, et al. Wan: Open and advanced large-scale video generative models. *arXiv preprint arXiv:2503.20314*, 2025. 3, 6

[60] Chaoyang Wang, Ashkan Mirzaei, Vedit Goel, Willi Menapace, Aliaksandr Siarohin, Avalon Vinella, Michael Vasilkovsky, Ivan Skorokhodov, Vladislav Shakhrai, Sergey Korolev, et al. 4real-video-v2: Fused view-time attention and feedforward reconstruction for 4d scene generation. *NeurIPS*, 2025. 3

[61] Chaoyang Wang, Peiye Zhuang, Tuan Duc Ngo, Willi Menapace, Aliaksandr Siarohin, Michael Vasilkovsky, Ivan Skorokhodov, Sergey Tulyakov, Peter Wonka, and Hsin-Ying Lee. 4real-video: Learning generalizable photo-realistic 4d video diffusion. In *Proceedings of the Computer Vision and Pattern Recognition Conference*, pages 17723–17732, 2025. 1, 3

[62] Fu-Yun Wang, Xiaoshi Wu, Zhaoyang Huang, Xiaoyu Shi, Dazhong Shen, Guanglu Song, Yu Liu, and Hongsheng Li. Be-your-outpainter: Mastering video outpainting through input-specific adaptation. In *European Conference on Computer Vision*, pages 153–168. Springer, 2024. 3

[63] Qianqian Wang, Zhicheng Wang, Kyle Genova, Pratul Srinivasan, Howard Zhou, Jonathan T. Barron, Ricardo Martin-

Brualla, Noah Snavely, and Thomas Funkhouser. Ibrnet: Learning multi-view image-based rendering. In *CVPR*, 2021. 3

[64] Ting-Chun Wang, Ming-Yu Liu, Jun-Yan Zhu, Guilin Liu, Andrew Tao, Jan Kautz, and Bryan Catanzaro. Video-to-video synthesis. *arXiv preprint arXiv:1808.06601*, 2018. 3

[65] Ting-Chun Wang, Ming-Yu Liu, Andrew Tao, Guilin Liu, Jan Kautz, and Bryan Catanzaro. Few-shot video-to-video synthesis. *arXiv preprint arXiv:1910.12713*, 2019. 3

[66] Zian Wang, Tianchang Shen, Merlin Nimier-David, Nicholas Sharp, Jun Gao, Alexander Keller, Sanja Fidler, Thomas Müller, and Zan Gojcic. Adaptive shells for efficient neural radiance field rendering. *ACM Trans. Graph.*, 42(6), 2023. 3

[67] Zhouxia Wang, Ziyang Yuan, Xintao Wang, Yaowei Li, Tianshui Chen, Menghan Xia, Ping Luo, and Ying Shan. Motionctrl: A unified and flexible motion controller for video generation. In *SIGGRAPH*, 2024. 2

[68] Daniel Watson, Saurabh Saxena, Lala Li, Andrea Tagliasacchi, and David J. Fleet. Controlling space and time with diffusion models. *arXiv preprint arXiv:2407.07860*, 2024. 2

[69] Rundi Wu, Ruiqi Gao, Ben Poole, Alex Trevithick, Changxi Zheng, Jonathan T Barron, and Aleksander Holynski. Cat4d: Create anything in 4d with multi-view video diffusion models. *arXiv preprint arXiv:2411.18613*, 2024. 3

[70] Rundi Wu, Ben Mildenhall, Philipp Henzler, Keunhong Park, Ruiqi Gao, Daniel Watson, Pratul P. Srinivasan, Dor Verbin, Jonathan T. Barron, Ben Poole, and Aleksander Holynski. ReconFusion: 3D reconstruction with diffusion priors. In *Proceedings of the IEEE/CVF Conference on Computer Vision and Pattern Recognition*, pages 21551–21561, 2024. 2, 3

[71] Yuxi Xiao, Qianqian Wang, Shangzhan Zhang, Nan Xue, Sida Peng, Yujun Shen, and Xiaowei Zhou. Spatialtracker: Tracking any 2d pixels in 3d space. In *Proceedings of the IEEE/CVF Conference on Computer Vision and Pattern Recognition*, pages 20406–20417, 2024. 3

[72] Zeqi Xiao, Wenqi Ouyang, Yifan Zhou, Shuai Yang, Lei Yang, Jianlou Si, and Xingang Pan. Trajectory attention for fine-grained video motion control. In *The Thirteenth International Conference on Learning Representations*, 2025. 3

[73] Yiming Xie, Chun-Han Yao, Vikram Voleti, Huaizu Jiang, and Varun Jampani. Sv4d: Dynamic 3d content generation with multi-frame and multi-view consistency. *arXiv preprint arXiv:2407.17470*, 2024. 3

[74] Dejia Xu, Weili Nie, Chao Liu, Sifei Liu, Jan Kautz, Zhangyang Wang, and Arash Vahdat. Camco: Camera-controllable 3d-consistent image-to-video generation. *arXiv preprint arXiv:2406.02509*, 2024. 1

[75] Yiran Xu, Taesung Park, Richard Zhang, Yang Zhou, Eli Shechtman, Feng Liu, Jia-Bin Huang, and Difan Liu. Videogigagan: Towards detail-rich video super-resolution. *arXiv preprint arXiv:2404.12388*, 2024. 3

[76] Jiawei Yang, Boris Ivanovic, Or Litany, Xinshuo Weng, Sung Wook Kim, Boyi Li, Tong Che, Danfei Xu, Sanja Fidler, Marco Pavone, and Yue Wang. Emernerf: Emergent spatial-temporal scene decomposition via self-supervision. *arXiv preprint arXiv:2311.02077*, 2023. 3

[77] Shuai Yang, Yifan Zhou, Ziwei Liu, and Chen Change Loy. Rerender a video: Zero-shot text-guided video-to-video translation. In *SIGGRAPH Asia 2023 Conference Papers*, pages 1–11, 2023. 3

[78] Shiyuan Yang, Liang Hou, Haibin Huang, Chongyang Ma, Pengfei Wan, Di Zhang, Xiaodong Chen, and Jing Liao. Direct-a-video: Customized video generation with user-directed camera movement and object motion. In *Special Interest Group on Computer Graphics and Interactive Techniques Conference Conference Papers '24 (SIGGRAPH Conference Papers '24)*, page 12, New York, NY, USA, 2024. ACM. 1

[79] Shiyuan Yang, Liang Hou, Haibin Huang, Chongyang Ma, Pengfei Wan, Di Zhang, Xiaodong Chen, and Jing Liao. Direct-a-video: Customized video generation with user-directed camera movement and object motion. In *ACM SIGGRAPH 2024 Conference Papers*, pages 1–12, 2024. 2

[80] Zhuoyi Yang, Jiayan Teng, Wendi Zheng, Ming Ding, Shiyu Huang, Jiazheng Xu, Yuanming Yang, Wenyi Hong, Xiaohan Zhang, Guanyu Feng, et al. Cogvideox: Text-to-video diffusion models with an expert transformer. *arXiv preprint arXiv:2408.06072*, 2024. 2, 3

[81] Meng You, Zhiyu Zhu, Hui Liu, and Junhui Hou. NVS-Solver: video diffusion model as zero-shot novel view synthesizer. *CoRR*, abs/2405.15364, 2024. 3

[82] Alex Yu, Vickie Ye, Matthew Tancik, and Angjoo Kanazawa. pixelNeRF: Neural radiance fields from one or few images. In *CVPR*, 2021. 3

[83] Mark YU, Wenbo Hu, Jinbo Xing, and Ying Shan. Trajectorycrafter: Redirecting camera trajectory for monocular videos via diffusion models. *arXiv preprint arXiv:2503.05638*, 2025. 2, 3, 6, 8, 9

[84] Mark YU, Wenbo Hu, Jinbo Xing, and Ying Shan. Trajectorycrafter: Redirecting camera trajectory for monocular videos via diffusion models, 2025. 8

[85] Wangbo Yu, Jinbo Xing, Li Yuan, Wenbo Hu, Xiaoyu Li, Zhipeng Huang, Xiangjun Gao, Tien-Tsin Wong, Ying Shan, and Yonghong Tian. ViewCrafter: taming video diffusion models for high-fidelity novel view synthesis. *arXiv preprint arXiv:2409.02048*, 2024. 2, 3

[86] Zehao Yu, Torsten Sattler, and Andreas Geiger. Gaussian opacity fields: Efficient adaptive surface reconstruction in unbounded scenes. *ACM Transactions on Graphics*, 2024. 3

[87] David Junhao Zhang, Roni Paiss, Shiran Zada, Nikhil Kannan, David E Jacobs, Yael Pritch, Inbar Mosseri, Mike Zheng Shou, Neal Wadhwa, and Nataniel Ruiz. Recapture: Generative video camera controls for user-provided videos using masked video fine-tuning. *arXiv preprint arXiv:2411.05003*, 2024. 3

[88] Junyi Zhang, Charles Herrmann, Junhwa Hur, Varun Jampani, Trevor Darrell, Forrester Cole, Deqing Sun, and Ming-Hsuan Yang. Monst3r: A simple approach for estimating geometry in the presence of motion. *arXiv preprint arXiv:2410.03825*, 2024. 3

[89] Guangcong Zheng, Teng Li, Rui Jiang, Yehao Lu, Tao Wu, and Xi Li. Cami2v: Camera-controlled image-to-video diffusion model. *arXiv preprint arXiv:2410.15957*, 2024. 2

- [90] Sixiao Zheng, Zimian Peng, Yanpeng Zhou, Yi Zhu, Hang Xu, Xiangru Huang, and Yanwei Fu. Vidcraft3: Camera, object, and lighting control for image-to-video generation. *arXiv preprint arXiv:2502.07531*, 2025. 2
- [91] Jensen Zhou, Hang Gao, Vikram Voleti, Aaryaman Vasishta, Chun-Han Yao, Mark Boss, Philip Torr, Christian Rupprecht, and Varun Jampani. Stable virtual camera: Generative view synthesis with diffusion models. *arXiv preprint arXiv:2503.14489*, 2025. 1, 2, 6, 8
- [92] Kun Zhou, Wenbo Li, Yi Wang, Tao Hu, Nianjuan Jiang, Xiaoguang Han, and Jiangbo Lu. NeRFLix: high-quality neural view synthesis by learning a degradation-driven inter-viewpoint mixer. In *CVPR*, pages 12363–12374, 2023. 3
- [93] Shangchen Zhou, Peiqing Yang, Jianyi Wang, Yihang Luo, and Chen Change Loy. Upscale-a-video: Temporal-consistent diffusion model for real-world video super-resolution. In *Proceedings of the IEEE/CVF Conference on Computer Vision and Pattern Recognition*, pages 2535–2545, 2024. 3
- [94] Tinghui Zhou, Richard Tucker, John Flynn, Graham Fyffe, and Noah Snavely. Stereo magnification: Learning view synthesis using multiplane images. *arXiv preprint arXiv:1805.09817*, 2018. 5

# ⚠️OMNIVIEW: An All-Seeing Diffusion Model for 3D and 4D View Synthesis

## Supplementary Material

### 6. Background: RoPE

RoPE [53] injects positional information into self-attention by *rotating* each 2D channel pair of the query and key vectors with sinusoidal, index-dependent phases. This rotation makes attention scores a function of relative displacement (via phase differences) rather than absolute indices, yielding a smooth decay with distance, translation equivariance of the dot-product, and strong length/extrapolation behavior—all without adding parameters. For video tokens, the position is naturally 3D  $(x, y, t)$ ; phases can be assigned per axis and combined (e.g., additively) to induce a spatio-temporal inductive bias. We use the shorthand  $\text{RoPE}(\mathbf{q}_{xyt}^z) = R(\mathbf{q}_{xyt}^z, \theta_{xyt})$  and apply the same operator to keys, where  $\theta_{xyt}$  denotes the sinusoidal phase parameters determined by  $(x, y, t)$ .

Let the token dimension be  $d$  and index  $J = d/2$  two-dimensional channel pairs by  $j = 0, \dots, J-1$ . For each axis  $a \in \{x, y, t\}$  define

$$\omega_j^{(a)} = B^{-2j/d}, \quad B = 10,000.$$

For a video position  $p = (x, y, t)$ , the per-pair phase is

$$\varphi_j(p) = x\omega_j^{(x)} + y\omega_j^{(y)} + t\omega_j^{(t)}, \quad \theta_{xyt} \equiv \{\varphi_j(p)\}_{j=0}^{J-1}.$$

Splitting a vector  $u \in \mathbb{R}^d$  into 2D slices  $u^{(j)} = (u_{2j}, u_{2j+1})^\top$  and rotating each slice gives us

$$R(u, \theta_{xyt})^{(j)} = \begin{bmatrix} \cos \varphi_j & -\sin \varphi_j \\ \sin \varphi_j & \cos \varphi_j \end{bmatrix} u^{(j)}, \quad \varphi_j = \varphi_j(p).$$

This is then applied to queries and keys from video latents  $z$ :

$$\hat{\mathbf{q}}_{xyt}^z = R(\mathbf{q}_{xyt}^z, \theta_{xyt}), \quad \hat{\mathbf{k}}_{xyt}^z = R(\mathbf{k}_{xyt}^z, \theta_{xyt}).$$

For positions  $m$  and  $n$ , the inner product depends only on the relative phase:

$$\langle \hat{\mathbf{q}}_m^z, \hat{\mathbf{k}}_n^z \rangle = \langle \mathbf{q}_m^z, R(\mathbf{k}_n^z, \{\varphi_j(n) - \varphi_j(m)\}_j) \rangle,$$

yielding a smooth relative spatio-temporal bias without added parameters.

### 7. Ablation with PRoPE

In addition to the ablations shown with different variants in Table 6 of the main paper, we compare with another variation of RoPE for camera control [32] (PRoPE). PRoPE consists of replacing the RoPE rotation matrix with the camera projection matrices for half of the dimensions while

Table 7. Ablation study comparing with PRoPE [32] on N3DV.

| Variant                 | PSNR↑        | SSIM↑        | LPIPS↓       |
|-------------------------|--------------|--------------|--------------|
| PRoPE                   | 12.39        | 0.358        | 0.648        |
| <b>Ours: + Attn Cat</b> | <b>15.46</b> | <b>0.376</b> | <b>0.456</b> |

reorganizing the other half for 2D  $xy$  coordinates. They, however, require training the diffusion model from initialization as opposed to our approach which utilizes existing trained video diffusion models. Nevertheless, we evaluate their approach in a finetuning setting using the pretrained video diffusion model. As they do not directly target the dynamic video setting, we extend their approach to modify the RoPE dimensions corresponding to the spatial coordinates while keeping the temporal dimensions as is. We train the model in this setting for 30K iterations and evaluate on the N3DV monocular video NVS task. Results are summarized in Tab. 7. We see that PRoPE leads to noisy reconstructions across all metrics likely due to the model incapable of significantly altering the underlying RoPE mechanism in the DiT, and can potentially require a large number of iterations for convergence. This is in contrast to our approach, which closely retains the 3D spatio-temporal RoPE structure, especially in the standard base setting of same cameras between different latents.

### 8. Qualitative visualizations

We now visualize the generations from our approach across a wide-variety of tasks

**Static multi-view NVS on LLFF.** We visualize the generations from our approach as well as Stable Virtual Camera (SEVA) [91] for the case of 3 conditioning views and compare it with the Ground-Truth (GT) across 5 scenes in LLFF. Results are shown in Fig. 6. We see that we consistently obtain higher quality generations while SEVA leads to blurrier outputs. We also obtain generations which are more aligned with the GT such as the tip of the fern (top row), or the flower (second from top row), or the legs of the dinosaur (bottom row). We also visualize the generations with increasing number of views in Fig. 7. With increasing multi-views as input, the model reduces scale ambiguity reconstructing the scene more faithfully while also incorporating appearance information from additional input views.

**T2V/I2V+Camera Control on RE10K.** We show qualitative results with Camera Control on RE10K with text (T2V) or image (I2V) conditions. I2V results are visual-

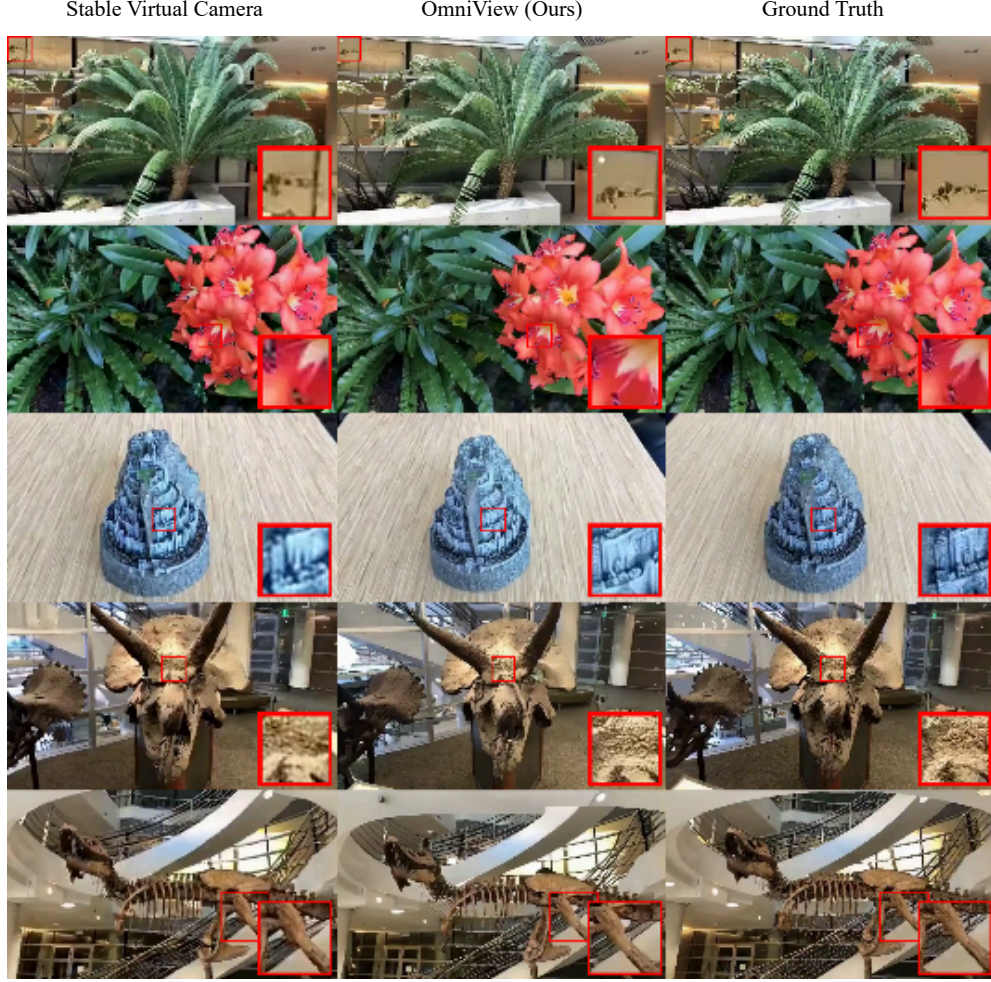


Figure 6. **Qualitative visualizations on the static multi-view NVS task on the LLFF dataset** Compared to Stable Virtual Camera [91], we obtain much higher detail along with aligned generations to the Ground-Truth, highlighted by the larger gap in SSIM values in Table 3 of the main paper.

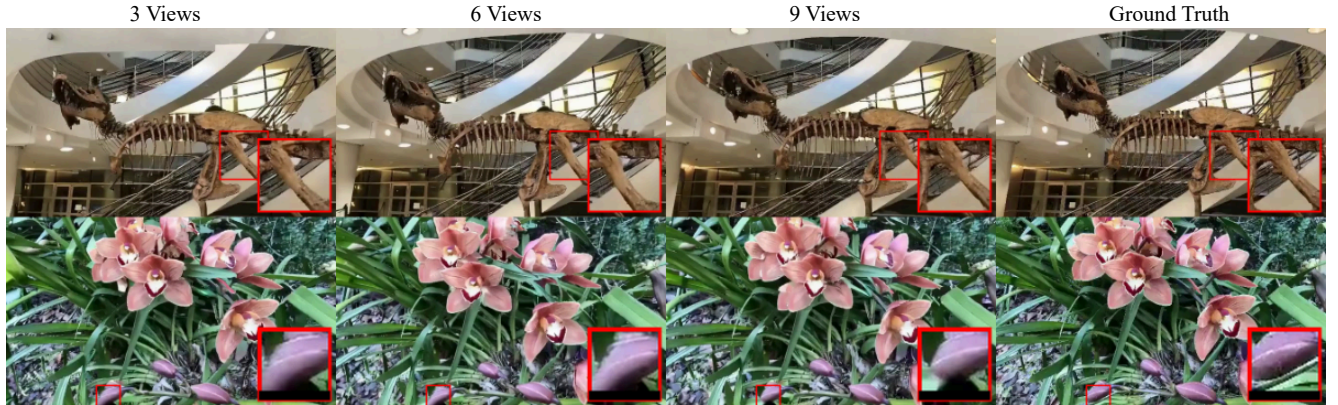


Figure 7. **Varying number of input views for static multi-view NVS.** We consistently improve upon our generations with increasing number of input conditioning views leading to reconstructions more aligned with the Ground-Truth.



Figure 8. **Qualitative visualizations on the I2V + Camera Control task on RE10K.** Compared to prior works of [51, 83], we obtain generations which are more 3D consistent with the input image condition and hence are better aligned with the Ground-Truth (Highlighted red boxes for example).

ized in Fig. 8. We see that compared to GEN3C or TrajectoryCrafter we more closely align with the input camera trajectory resulting in generations which are better aligned with the GT view. We highlight certain regions with red boxes such as the door in the first column, or the photo frame in the last column showing generations with reference to the GT. We also produce realistic hallucinations in new regions unseen in the input view, while largely maintaining 3D consistency with the regions visible in the input. Next, we compare the camera control performance for the T2V setting with AC3D [2]. Results are shown in Fig. 9. We utilize the camera trajectory from a source video and generate new videos with this trajectory. We see that AC3D can significantly deviate from the source trajectory, such as the zooming in for the first scene while AC3D rotates left. We on the hand, are consistent with the camera input equivalently zooming into the scene. A similar but inverse result is observed in the third scene where the input camera slightly pans/rotates left while AC3D produces a zoomed in version, while we produce generations consistent with this trajectory.

**Monocular Video NVS on DAVIS.** We now show results for the monocular video NVS task on DAVIS. Results are visualized in Fig. 10 comparing with GEN3C and Recammaster. We show 3 target trajectories from top to bottom for the 3 scenes: a) Translating right while looking to the left) b) Translating down while looking up and c) Translating left while looking to the right. The input trajectory can vary depending on the scene. We see that we consistently obtain clean generations. For the first scene, we are right showing a slightly frontal view of the swan while GEN3C produces significant deformations and Recammaster mainly translates with little rotation. Both approaches also fail for the second scene resulting in significantly high artifacts in the generation inconsistent with the input. For the 3rd view with the target trajectory close to the input trajectory, we produce relatively clean generations with fewer artifacts close to the bus.

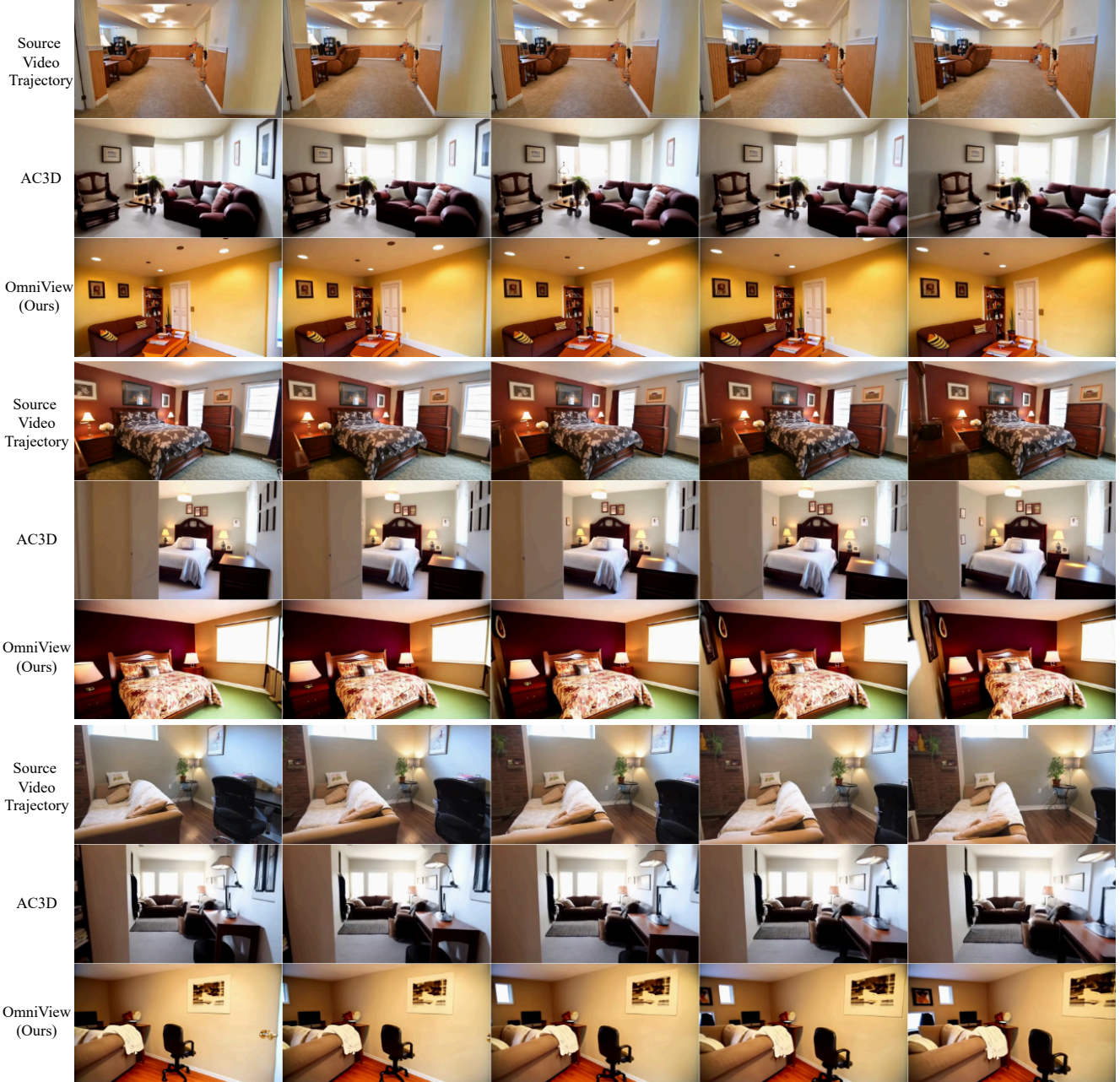


Figure 9. **Qualitative visualizations on the T2V + Camera Control task on RE10K.** Compared to AC3D [2], we obtain generations which follow the camera trajectory in the source video while also producing high-fidelity video generations.

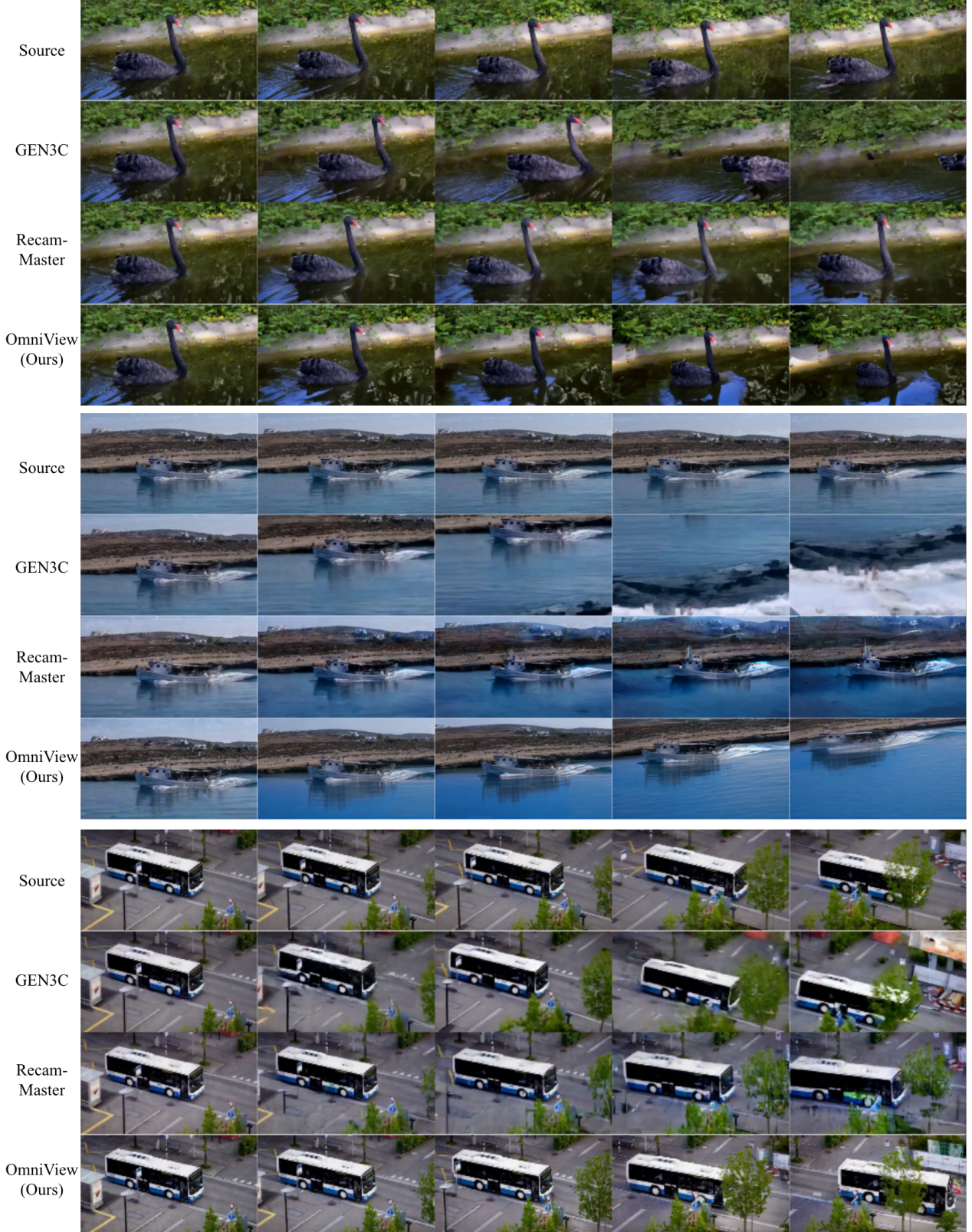


Figure 10. **Video NVS generations on DAVIS.** We visualize generated videos with new trajectories compared to the source video. We obtain generations which are more trajectory consistent (top, middle), and also higher fidelity generations (bottom) with fewer artifacts.